Ab initio potential energy surfaces for NH($^3\Sigma^-$) – NH($^3\Sigma^-$) with analytical long range

Liesbeth M. C. Janssen, Gerrit C. Groenenboom, and Ad van der Avoird*

Theoretical Chemistry, Institute for Molecules and Materials (IMM),

Radboud University Nijmegen, Heyendaalseweg 135,

6525 AJ Nijmegen, The Netherlands

Piotr S. Żuchowski

Department of Chemistry, Durham University,

South Road, DH1 3LE, United Kingdom

Rafał Podeszwa

Institute of Chemistry, University of Silesia,

Szkolna 9, 40-006 Katowice, Poland

(Dated: September 18, 2009)

Abstract

We present four-dimensional *ab initio* potential energy surfaces for the three different spin states of the NH($^3\Sigma^-$) – NH($^3\Sigma^-$) complex. The potentials are partially based on the work of Dhont *et al.* [J. Chem. Phys. **123**, 184302 (2005)]. The surface for the quintet state is obtained at the RCCSD(T)/aug-cc-pVTZ level of theory and the energy differences with the singlet and triplet states are calculated at the CASPTn/aug-cc-pVTZ ($n = 2, 3$) level of theory. The *ab initio* potentials are fitted to coupled spherical harmonics in the angular coordinates, and the long range is further expanded as a power series in $1/R$. The RCCSD(T) potential is corrected for a size-consistency error of about 0.5×10^{-6} E_h prior to fitting. The long-range coefficients obtained from the fit are found to be in good agreement with first and second-order perturbation theory calculations.

*Electronic mail: A.vanderAvoird@theochem.ru.nl

I. INTRODUCTION

The field of cold ($T < 1$ K) and ultracold (< 1 mK) molecules has attracted great interest in the last few years. The production of such (ultra)cold species may find important applications in condensed matter physics [1], high precision spectroscopy [2, 3, 4], physical chemistry [5, 6, 7, 8, 9], and quantum computing [10, 11]. There are, in principle, two different strategies for producing molecular samples at (ultra)low temperatures. In indirect methods, cold molecules are formed by pairing up atoms that are already cooled down to the ultracold regime. Examples of such methods include photoassociation [12] and Feshbach association [13]. Conversely, direct methods such as Stark deceleration [14] and buffer gas cooling [15] employ a scheme in which pre-existing molecules are cooled down from higher temperatures.

One of the most promising candidates for direct-cooling experiments is the NH radical. NH($X\,^3\Sigma^-$) has a relatively large magnetic moment of 2 μ_B, making it suitable for buffer gas cooling and magnetic trapping experiments [8, 16, 17, 18]. Furthermore, the metastable $a\,^1\Delta$ state of NH, which exhibits a linear Stark effect, can be efficiently Stark decelerated and trapped in an electrostatic field. Subsequent excitation of the $A\,^3\Pi \leftarrow a\,^1\Delta$ transition followed by spontaneous emission to the ground state yields cold NH($X\,^3\Sigma^-$) molecules, which in turn may be trapped in a magnetic field [19, 20]. This scheme also allows for reloading of the magnetic trap, thus providing a means to increase phase-space density.

At present, direct-cooling methods for NH are limited to temperatures of a few hundred mK. If the density of trapped molecules is sufficiently high, it may be possible to reach the ultracold regime by means of evaporative cooling. This process relies on elastic NH + NH collisions as the trap depth is gradually reduced. Inelastic spin-changing collisions between trapped NH molecules will lead to immediate trap loss and are therefore unfavorable. It is generally accepted that, in order for evaporative cooling to be successful, elastic collisions should be a few orders of magnitude more efficient than inelastic transitions [15, 16, 17, 21, 22]. In the case of NH($X\,^3\Sigma^-$), the only magnetically trappable state is the low-field seeking $M_S = 1$ state, with M_S denoting the spin projection quantum number. A collision complex of two such molecules is in the $M_S = 2$ level of the NH–NH high-spin quintet ($S = 2$) state. Inelastic collisions between NH molecules may either change the M_S quantum number of the quintet state, or change the total spin S to produce singlet or triplet complexes. The $S = 0$

and 1 dimer states are chemically reactive [23, 24] and, although unfavorable for evaporative cooling, could be of interest in the context of cold controlled chemistry [9].

A recent theoretical study by Kajita [25], in which only the electric dipole-induced dipole and magnetic dipole-dipole interactions were considered, showed that evaporative cooling of NH is likely to be feasible. A more rigorous quantum calculation of elastic and inelastic cross sections, however, requires knowledge of the full NH–NH interaction potentials for all three spin states. In particular the long-range potential, which governs the dynamics at (ultra)low temperatures, should be described very accurately. For NH–NH the dominant long-range term is the electrostatic dipole-dipole interaction, which scales with the intermolecular distance R as R^{-3}. If, however, the molecules are freely rotating, all multipole-multipole terms average out to zero and the isotropic (R^{-6}) dispersion and induction interactions become important.

Dhont *et al.* [26] have recently constructed four-dimensional *ab initio* potential energy surfaces for NH–NH which, in principle, contain all relevant long range contributions. They employed the partially spin-restricted coupled-cluster method with single and double excitations and a perturbative treatment of triples [RCCSD(T)] [27, 28] to obtain the surface for the NH–NH quintet state. We found, however, that this surface exhibits erroneous behavior in the long range due to a lack of size consistency in the open-shell RCCSD(T) method. In the present paper, we report more accurate *ab initio* calculations that are corrected for this undesirable feature, and which allow for an analytical fit of the long-range potential. The fit of the short-range potentials is also improved.

This paper is organized as follows. In Section II A, we first address the RCCSD(T) size-consistency problem and present new RCCSD(T) calculations for the long range of the NH–NH potential. Long-range perturbation theory calculations are discussed in Section II B, and new CASPTn ($n = 2, 3$) calculations for the short range of the singlet and triplet potentials are presented in Section II C. The fit of the different potentials is described in Section III, followed by a discussion of the results in Section IV. Finally, conclusive remarks are given in Section V.

II. ELECTRONIC STRUCTURE CALCULATIONS

A. RCCSD(T) potential energy surface

The coupled-cluster (CC) approach is one of the most accurate *ab initio* methods available for calculating potential energy surfaces. This method requires a single Slater determinant function as the reference state, which in the case of NH–NH implies that only the high-spin quintet state is suitable for coupled-cluster calculations. At large intermolecular distances however, the energy splittings between the three different spin states become negligible, and thus the CC potential also applies to the singlet and triplet states at long range. In this section, we will show that the previously reported NH–NH RCCSD(T) potential [26] contains a size-consistency error that becomes apparent at large R. We also present new *ab initio* calculations that are corrected for this defect. The coordinates used to describe the NH–NH potential energy surfaces are the four intermolecular Jacobi coordinates (R, θ_A, θ_B, ϕ). The coordinate R is the length of the intermolecular vector $\boldsymbol{R}$ that connects the centers of mass of monomers A and B, θ_A and θ_B are the polar angles of the NH monomer axes relative to $\boldsymbol{R}$, and ϕ is the dihedral angle between the planes through $\boldsymbol{R}$ and the monomer axes (see also Fig. 1 of Ref. [26]). All interaction potentials are computed using the supermolecule approach with the counterpoise correction method of Boys and Bernardi [29].

1. *Size consistency*

It is well established that coupled-cluster theory for closed-shell systems is rigorously size-consistent. For open-shell species, however, where the problem of nonzero spin arises, this issue is not straightforward. It was demonstrated in 2006 by Heckert *et al.* [30] that several spin-adapted CCSD schemes applied to the triplet F(^2P) – F(^2P) system exhibit size-consistency errors on the order of 10^{-7} – 10^{-8} E_h. The reason for this is still unclear, but it has been suggested that the problem lies in the truncation of the cluster operator [30]. Although the errors are very small, the effect becomes apparent when considering interactions at low temperatures, where the total energy of the system may be of a similar order of magnitude (10^{-7} $E_h \approx 0.03$ K). Hence, a lack of size consistency imposes a significant limitation on the accuracy of calculations in the (ultra)cold regime.

When evaluating the NH($^3\Sigma^-$) – NH($^3\Sigma^-$) quintet potential of Ref. [26] in more detail,

we indeed found that the interaction energy does not tend to zero at large intermolecular distances. At $R = 30\,000\ a_0$, the size-consistency error is $-4.8823 \times 10^{-6}\ E_h$ calculated at the RCCSD level of theory with the augmented correlation-consistent polarized valence triple-zeta (aug-cc-pVTZ) basis set [31], and $+0.5129 \times 10^{-6}\ E_h$ at the RCCSD(T)/aug-cc-pVTZ level of theory. It should be noted that these errors are independent of the relative orientation of the monomers, i.e., the lack of size consistency affects only the isotropic part of the potential. The results for other basis sets are given in Table I. It can be seen that the error is largest at the RCCSD level and increases with the size of the basis set. The inclusion of triple excitations reduces the error by approximately one order of magnitude and, for most basis sets, also changes its sign.

Although the problem has not been solved yet, we found that the NH–NH RCCSD(T) potential can be easily corrected for the lack of size consistency by simply subtracting the error, calculated at $30\,000\ a_0$, from all *ab initio* points. We compared these corrected energies with the results obtained from a spin-unrestricted CCSD(T) [UCCSD(T)] calculation, of which the energies do converge to zero at long range [i.e. UCCSD(T) is size-consistent]. At $R = 30.0\ a_0$, the root-mean-square (RMS) difference between the UCCSD(T) and corrected RCCSD(T) data was calculated to be $9.1\times10^{-9}\ E_h$ (0.08% of the mean absolute value of the potential) for a grid of 126 *ab initio* points. Without the size-consistency correction this difference would be $5.1\times10^{-7}\ E_h$ (4.4%). Thus, the error subtraction at the RCCSD(T) level leads to significantly better agreement with the size-consistent UCCSD(T) method. Similar results were obtained at an intermolecular distance of $15.0\ a_0$, where the RMS difference between the corrected RCCSD(T) and UCCSD(T) data is $7.0\times10^{-8}\ E_h$ (0.07% of the mean absolute energy), as opposed to $5.4\times10^{-7}\ E_h$ (0.54%) without the correction. At even smaller distances, the size-consistency error will become increasingly negligible compared to the total interaction energy, thus the correction will leave the short-range potential essentially unaffected. Based on these findings, we conclude that subtracting the error from all RCCSD(T) points does not significantly alter the accuracy of the potential, but does give the desired asymptotic behavior at long range.

2. *Long-range RCCSD(T) calculations*

Although the size-consistency correction already constitutes an important refinement to the RCCSD(T) potential of Ref. [26], we chose to improve the long range even further by performing new *ab initio* calculations. This is motivated by our aim to study collisions in the limit of zero temperature, for which it is desirable to have the long range in analytical form. In order to perform an accurate analytical fit, however, we found that the long-range *ab initio* energies should be converged to less than 10^{-10} E_h, while the data presented in Ref. [26] have been converged to only 10^{-8} E_h. We therefore recalculated the points at large R with much tighter convergence thresholds, as low as 10^{-13} E_h, to ensure that the fit will not be affected by numerical noise. The radial grid consisted of 8 points, approximately logarithmically spaced at 8.3, 10.0, 12.0, 14.4, 17.3, 20.8, 25.0, and 30.0 a_0. For the angular grid, we chose an 11-point Gauss-Legendre quadrature grid in (θ_A, θ_B) and an 11-point Gauss-Chebyshev grid in ϕ. These are known to be the most accurate quadratures on their respective domains [32]. Due to the symmetry of the complex, only points with $\theta_A + \theta_B \leq \pi$ and $0 \leq \phi \leq \pi$ were required in the calculations [26]. The monomers were treated as rigid rotors, with the NH bond length fixed to the experimental equilibrium value of 1.0362 Å [33]. The RCCSD(T) energies were computed using the aug-cc-pVTZ basis set, with additional bond functions located at the midpoint of the intermolecular vector $\boldsymbol{R}$ (exponents s, p: 0.9, 0.3, and 0.1; d, f: 0.6 and 0.2; g: 0.3). All calculations were performed with the MOLPRO package [34]. As explained above, the size-consistency error of 0.51290×10^{-6} E_h was subtracted from all RCCSD(T) points to ensure that the long range converges to zero.

B. Perturbation theory calculations

As an additional test for the accuracy of the RCCSD(T) long-range potential, we computed the long-range coefficients directly from first and second-order perturbation theory with the multipole expansion of the interaction operator (see e.g. Ref. [35]). The first-order (electrostatic) coefficients are expressed in terms of the permanent NH multipole moments, while the second-order (induction and dispersion) coefficients depend also on the static and dynamic polarizabilities of NH. The permanent multipole moments were obtained from finite field calculations at the RCCSD(T)/aug-cc-pVTZ level of theory and from density

functional theory (DFT), yielding two different sets of first-order coefficients. All DFT calculations were performed with the PBE0 density functional [36] and the aug-cc-pVQZ basis set. The Kohn-Sham orbitals were obtained from a spin-restricted calculation using the DALTON program [37]. The Fermi-Amaldi asymptotic correction [38] was employed to improve the description of the NH densities. The ionization potentials used for this correction were taken from Ref. [39]. For the static and dynamic NH polarizabilities, we performed spin-restricted time-dependent coupled Kohn-Sham (CKS) calculations [39]. Previous studies have shown that CKS methods yield accurate van der Waals coefficients, comparable to the accuracies obtained with the best *ab initio* methods, for systems such as He_2, Ne_2, H_2O dimer [40], and the open-shell O_2 dimer [41]. The static polarizabilities and dynamic polarizabilities at imaginary frequencies were obtained with a modified version of the SAPT2008 package [42], extended to treat open-shell fragments. Finally, the second-order long-range coefficients were computed from the DFT multipole moments and response functions using the POLCOR program [43].

C. CASPTn calculations

As mentioned before, the RCCSD(T) quintet potential can also be used to describe the singlet and triplet NH–NH states at long range. In the short range, however, these lower-spin states must be treated with a different *ab initio* method. Dhont *et al.* [26] employed the Complete Active Space with nth-order Perturbation Theory (CASPTn) method ($n = 2, 3$) to calculate the energy differences between the quintet state and the $S = 0$ and 1 states, and added those to the RCCSD(T) quintet surface to obtain the singlet and triplet potentials:

$$V_n^S = V_{CASPTn}^S - V_{CASPTn}^{S=2} + V_{RCCSD(T)}^{S=2}. \tag{1}$$

When fitting the CASPTn energy splittings, which decay exponentially as a function of R, we found that the convergence thresholds used in Ref. [26] were not sufficiently stringent to reach the same accuracy as in the long range. Hence, we recalculated the CASPTn energies for all three spin states with much tighter convergence criteria. The active space consisted of the four orbitals that are singly occupied in the quintet state. The g_4 operator [44] was used to obtain size-consistent results, and a level shift of 0.4 was applied to enforce convergence. The interaction energies were computed for R = 4.0, 4.5, 5.0, 5.5, 6.0, 6.5, 7.0, 7.5, 8.0, 8.5,

9.0, 10.0, 12.0, and 14.4 a_0, with the energy threshold set to 10^{-13} E_h for the points at 8.0 – 14.4 a_0, 10^{-12} E_h at 7.0 and 7.5 a_0, 10^{-11} E_h at 6.0 and 6.5 a_0, 10^{-10} E_h at 5.0 and 5.5 a_0, 10^{-9} E_h at 4.5 a_0, and 10^{-8} E_h at 4.0 a_0. For the angular grid we used the same points as for the long-range RCCSD(T) calculations, i.e. an 11-point Gauss-Legendre quadrature in (θ_A, θ_B) and an 11-point Gauss-Chebyshev grid in ϕ. The CASPTn calculations were performed with MOLPRO [34] using the aug-cc-pVTZ basis set supplemented with bond functions. It should be noted that three points at 4.0 a_0 failed to converge due to the strongly repulsive nature of the potential at small R.

III. ANALYTICAL REPRESENTATION

All three interaction potentials can be represented as follows:

$$V(R,\theta_A,\theta_B,\phi) = \sum_{L_A,L_B,L} v_{L_A,L_B,L}(R) A_{L_A,L_B,L}(\theta_A,\theta_B,\phi) \tag{2}$$

$$= \sum_{L_A,L_B,M} v_{L_A,L_B,M}(R) A_{L_A,L_B,M}(\theta_A,\theta_B,\phi). \tag{3}$$

The angular functions $A_{L_A,L_B,L}(\theta_A,\theta_B,\phi)$ are defined as

$$A_{L_A,L_B,L}(\theta_A,\theta_B,\phi) = \sum_{M=-\min(L_A,L_B)}^{\min(L_A,L_B)} \begin{pmatrix} L_A & L_B & L \\ M & -M & 0 \end{pmatrix} C_{L_A,M}(\theta_A,\phi_A) C_{L_B,-M}(\theta_B,\phi_B),$$

$$= \sum_{M=0}^{\min(L_A,L_B)} (-1)^M \begin{pmatrix} L_A & L_B & L \\ M & -M & 0 \end{pmatrix} A_{L_A,L_B,M}(\theta_A,\theta_B,\phi), \tag{4}$$

where $C_{L,M}(\theta,\phi)$ are Racah-normalized spherical harmonics and $\phi = \phi_A - \phi_B$ is the difference between the azimuthal angles of monomers A and B. The factor in brackets denotes a Wigner three-j symbol. The 'primitive' angular functions $A_{L_A,L_B,M}(\theta_A,\theta_B,\phi)$ are given by

$$A_{L_A,L_B,M}(\theta_A,\theta_B,\phi) = P_{L_A,M}(\cos\theta_A) P_{L_B,M}(\cos\theta_B) \cos M\phi, \tag{5}$$

where $P_{L,M}(\cos\theta)$ are Schmidt semi-normalized associated Legendre functions defined in Ref. [26]. The R-dependent expansion coefficients are related to each other as [26]

$$v_{L_A,L_B,L}(R) = (2L+1) \sum_{M=0}^{\min(L_A,L_B)} (-1)^M (2-\delta_{M0}) \begin{pmatrix} L_A & L_B & L \\ M & -M & 0 \end{pmatrix} v_{L_A,L_B,M}(R). \tag{6}$$

A. Long-range potential

For the analytical long-range interaction, we use Eq. (2) and further expand the $v_{L_A,L_B,L}(R)$ coefficients in a power series in $1/R$:

$$v_{L_A,L_B,L}(R) = \sum_n \frac{-C_{L_A,L_B,L,n}}{R^n}. \tag{7}$$

Our choice of an 11-point Gauss-Legendre quadrature in (θ_A, θ_B) and an 11-point Gauss-Chebyshev quadrature in ϕ ensures that the angular $A_{L_A,L_B,L}$ functions, when evaluated on the quadrature grid with the appropriate weights, are mutually orthogonal for all values of L_A and L_B up to 10 inclusive. Thus, we can perform the analytical fit in R [Eq. (7)] for each (L_A, L_B, L) term separately. The values of n follow from a consideration of the possible first-order (electrostatic) and second-order (induction/dispersion) contributions (see e.g. Ref. [45] for details). For the electrostatic terms, we have $L_A + L_B = L$ and $n = L_A + L_B + 1$, with $L_A \geq 1$ and $L_B \geq 1$. The minimum value of 1 comes from the fact that the lowest nonvanishing permanent multipole moment of NH is the dipole. In the case of induction and dispersion interactions, L_A and L_B correspond to the order of two coupled multipole moments on monomers A and B, respectively. That is, $L_A = |l_A - l'_A|, \ldots, l_A + l'_A$ and $L_B = |l_B - l'_B|, \ldots, l_B + l'_B$, where l_A, l'_A, l_B, and l'_B denote the orders of the uncoupled monomer multipole moments. L_A and L_B are in turn coupled to all possible L values, and for each (L_A,L_B,L) term we have $n = l_A + l'_A + l_B + l'_B + 2$. Finally, due to the inversion symmetry of the total system, it can be shown that $L_A + L_B + L$ is even, and since each monomer is a linear Σ state molecule, $l_A + l'_A + L_A$ and $l_B + l'_B + L_B$ must also be even [45].

The $C_{L_A,L_B,L,n}$ fit coefficients of Eq. (7) were calculated as follows. For each set of (L_A, L_B, L) values, we first computed the lowest possible values of n in both first and second order. Since our long-range *ab initio* calculations were performed on a grid of eight R points, we could include a maximum of eight R^{-n} functions in the fit. We then fitted the size-consistency corrected RCCSD(T) data to the expansion of Eq. (2), and subsequently fitted each $v_{L_A,L_B,L}$ expansion coefficient in terms of R^{-n} functions [Eq. (7)]. Note that the fit of Eq. (2) is mathematically equivalent to evaluating the overlap integral between the angular functions and $V(R, \theta_A, \theta_B, \phi)$ by Gauss-Legendre quadrature. The fit was done using a linear least-squares procedure in which the *ab initio* points were weighted with the appropriate quadrature weights and a factor of R^3. The R-dependent factor is chosen

because the leading dipole-dipole interaction decays as R^{-3}.

In principle, our long-range expansion is valid for all terms up to $L_A = L_B = 10$, with eight possible values of n for each (L_A, L_B, L) term. However, the inclusion of high powers of $1/R$ may lead to unphysical results even for the low-n coefficients, which are considered the most important. Thus, we must carefully choose which $R^{-n} A_{L_A,L_B,L}(\theta_A, \theta_B, \phi)$ functions to include in the fit. After extensive testing, we found that the best analytical fit is obtained for $n \leq 14$. This result is based on a thorough examination of both the stability of the fit, i.e. how much the $C_{L_A,L_B,L,n}$ coefficients vary when adding more R^{-n} functions, and the RMS error in the data points. The final fit gave a RMS error of 4.6×10^{-8} E_h (0.03%) for a total of 10648 *ab initio* points. The RMS difference between the analytical potential and the size-consistency corrected long-range points of Ref. [26], which served as test points, was 4.8×10^{-7} E_h (0.24%). Note that the latter error is, in part, due to the weaker convergence thresholds used in the calculations of Ref. [26]. The $C_{L_A,L_B,L,n}$ fit coefficients are available through EPAPS [46].

B. Short-range $S = 2$ potential

For the short range of the quintet surface, we used the size-consistency corrected RCCSD(T) data of Dhont *et al.* [26], calculated at R values from 4.0 to 16.0 a_0. The angular grid consisted of 11 points in θ_A and θ_B, ranging from 0° to 180° in steps of 20° with an additional point at 90°. The grid in ϕ ranged from 0° to 180° in steps of 22.5°. The short-range potential was first expanded in terms of $A_{L_A,L_B,M}(\theta_A, \theta_B, \phi)$ functions [Eq. (3)] and then transformed to Eq. (2). Instead of using the two-step spline-based approach described in Ref. [26], we employed a weighted least squares fitting procedure to determine the $v_{L_A,L_B,M}(R)$ coefficients for each R. In order to perform the fit, we first calculated optimal quadrature weights for the grid points in (θ_A, θ_B), of which the details are given in the Appendix. We then attempted to fit the RCCSD(T) points by an expansion in terms of $A_{L_A,L_B,M}(\theta_A, \theta_B, \phi)$ functions, weighting each point with the appropriate quadrature weights. High-energy points (> 0.1 E_h), which are not of practical importance in bound-state and scattering calculations, were excluded from the fit. It was found, however, that the least squares problem of Eq. (3) is ill-conditioned for $\max(L_A, L_B) \geq 9$ due to both the choice of grid points (the angle ϕ is undefined if θ_A or θ_B equals 0° or 180°) and the omission of

points at high energies. We therefore employed a modified fitting scheme to regularize the least squares problem such that all functions up to $L_A = L_B = 10$ and $M = 8$ could be included. This was done by means of a Tikhonov regularization method [47] in which the term $\sum_{L_A,L_B,M} |\alpha(L_A^2 + L_B^2) v_{L_A,L_B,M}(R)|^2$ was added to the residual. The factor of $\alpha(L_A^2 + L_B^2)$, with $\alpha = 2 \times 10^{-4}$, ensures that strong oscillations (associated with large L_A and L_B) are damped out in the fit. The resulting $v_{L_A,L_B,M}(R)$ fit coefficients were then transformed to $v_{L_A,L_B,L}(R)$ coefficients using Eq. (6). Overall, this fitting procedure gave a RMS error of $9.8{\times}10^{-6}$ E_h (0.21%) based on 21275 *ab initio* points. The $v_{L_A,L_B,L}(R)$ coefficients can be retrieved via the EPAPS system [46].

The $v_{L_A,L_B,L}(R)$ expansion coefficients were interpolated in R using the reproducing kernel Hilbert space (RKHS) method with the reproducing kernel for distancelike variables [48, 49]. The RKHS parameter m, which determines the power with which the interpolated function decays between the grid points, was set to the leading power in $1/R$ for each (L_A, L_B, L) term. For instance, the $v_{112}(R)$ coefficient containing the electrostatic dipole-dipole interaction was interpolated with $m = 3$, the isotropic $v_{000}(R)$ term was interpolated with $m = 6$, and so on. In all cases, the RKHS smoothness parameter was set to 2.

Finally, we matched the short-range and long-range expansions of the RCCSD(T) quintet potential using an R-dependent switching function $f(R)$ that changes smoothly from 0 to 1 on the interval $a < R < b$:

$$f(R) = \begin{cases} 0 & \text{if } R \le a \\ 1 & \text{if } R \ge b \\ \frac{1}{2} + \frac{1}{4} \sin \frac{\pi x}{2} \left(3 - \sin^2 \frac{\pi x}{2}\right) & \text{otherwise,} \end{cases} \tag{8}$$

with $x = \frac{(R-b)+(R-a)}{b-a}$. The function is such that the first three derivatives at $R = a$ and $R = b$ are zero. We used Eq. (8) to switch the potential between $a = 8$ and $b = 12$ a_0. The total $S = 2$ potential energy surface may now be expressed as follows:

$$V(R, \theta_A, \theta_B, \phi) = [1 - f(R)] V_{sr}(R, \theta_A, \theta_B, \phi) + f(R) V_{lr}(R, \theta_A, \theta_B, \phi), \tag{9}$$

where V_{sr} refers to the short-range expansion of Eq. (2) and V_{lr} to the long-range expansion of Eqs. (2) and (7).

C. Short-range $S = 0, 1$ potentials

As already mentioned in Section II, the singlet and triplet potentials were obtained from the quintet RCCSD(T) potential by adding the energy differences at the CASPT2 or CASPT3 level of theory. We fitted these exchange splittings ($V^S_{CASPTn} - V^{S=2}_{CASPTn}$) directly in terms of $A_{L_A,L_B,L}(\theta_A, \theta_B, \phi)$ functions, weighting each point with the corresponding Gauss-Legendre and Gauss-Chebyshev quadrature weights. In all cases, the fit error was largest at 4.0 a_0 and rapidly decreased as a function of R. For instance, the RMS errors for the singlet-quintet CASPT2 and CASPT3 splittings were 1.3×10^{-3} E_h (4.6%) and 1.2×10^{-3} E_h (4.7%) at 4.0 a_0, 1.1×10^{-5} E_h (0.10%) and 7.8×10^{-6} E_h (0.09%) at the neighboring grid point of 4.5 a_0, and 2.3×10^{-8} E_h (0.007%) and 1.9×10^{-8} E_h (0.007%) near the van der Waals minimum at 6.5 a_0. For the triplet-quintet CASPT2 and CASPT3 exchange splittings, the RMS errors were 6.9×10^{-4} E_h (3.2%) and 7.9×10^{-3} E_h (4.4%) at 4.0 a_0, 4.3×10^{-6} E_h (0.06%) and 5.1×10^{-6} E_h (0.08%) at 4.5 a_0, and 2.1×10^{-8} E_h (0.01%) and 6.0×10^{-8} E_h (0.03%) at 6.5 a_0. All errors were calculated from 1331 *ab initio* points per R value, with the exception of $R = 4.0$ a_0, where three points failed to converge. The $v_{L_A,L_B,L}(R)$ fit coefficients for the CASPTn energy splittings are available through EPAPS [46].

The $v_{L_A,L_B,L}(R)$ coefficients were interpolated in R using the RKHS method. For all (L_A, L_B, L) terms we set the RKHS parameter m to 14 and the smoothness parameter to 2. The value of $m = 14$ ensures that all coefficients decay as R^{-15} beyond the outermost grid point, thus decaying faster than any of the long-range terms included in the fit of Eq. (7). In addition, we found that the interpolation with $m = 14$ gives the smallest RMS error in the *ab initio* points of Ref. [26]. The expanded CASPTn splittings were added to the RCCSD(T) potential of Eq. (9) to obtain the final singlet and triplet potential energy surfaces.

IV. RESULTS AND DISCUSSION

The main features of the singlet, triplet, and quintet potentials have already been described in Ref. [26], and therefore we only briefly mention them here. Our $S = 2$ potential is characterized by a van der Waals minimum at $R_e = 6.61$ a_0 with a well depth of $D_e = -675$ cm^{-1}. It should be noted that Dhont *et al.* [26] reported a slightly different R_e value of 6.60

a_0. The minimum corresponds to a linear geometry ($\theta_A = \theta_B = \phi = 0°$) in which the two NH dipoles are aligned. Żuchowski *et al.* [39] have recently shown that D_e changes to -693 cm^{-1} if the aug-cc-pVQZ basis is used and the RCCSD(T) calculations are performed without the frozen-core approximation. They also demonstrated from symmetry-adapted perturbation theory (SAPT) calculations that the main contributions to D_e are the electrostatic (-899 cm^{-1}) and dispersion (-432 cm^{-1}) interactions. The total SAPT exchange-repulsion energy at the minimum was found to be 874 cm^{-1} [39].

The $V_2^{S=0}$ ($V_3^{S=0}$) and $V_2^{S=1}$ ($V_3^{S=1}$) surfaces also exhibit a van der Waals minimum at $\theta_A = \theta_B = \phi = 0°$, located at $R_e = 6.50$ (6.51) and 6.54 (6.55) a_0, respectively. These distances are 0.01 – 0.02 a_0 different from the R_e values reported by Dhont *et al.* [26]. Furthermore, the singlet and triplet dimers may form the chemically stable N_2H_2 molecule, which is reflected in the strongly attractive nature of these potentials at short intermolecular separations. The most favorable geometries for the $S = 0$ and 1 states at short distances are found near $\theta_A = \theta_B = 90°$.

A. Long-range potential

Before discussing the analytical fit results, we first address the size-consistency problem occurring at the RCCSD and RCCSD(T) levels of theory. Figure 1 shows the isotropic part of the quintet potential, $v_{000}(R)$, between $R = 15$ and 30 a_0. The lack of size consistency is most apparent at the RCCSD level, giving rise to an error of -1.07 cm^{-1} at long range. The inclusion of triple excitations reduces the problem significantly, but in fact overcompensates for the RCCSD error by $+0.11$ cm^{-1}. The uncorrected isotropic RCCSD and RCCSD(T) potentials cross at $R \approx 11$ a_0. After subtracting the size-consistency errors from all *ab initio* points, both the RCCSD and RCCSD(T) potentials smoothly converge to zero at long range. It can also be seen that these corrected data are in very good agreement with the corresponding spin-unrestricted CC results at $R = 15$ and 30 a_0.

The main fit results for the (size-consistency corrected) RCCSD(T) long-range potential are presented in Table II. A total number of 588 $C_{L_A,L_B,L,n}$ coefficients was included in the long-range fit ($L_A, L_B \leq 10$ and $n \leq 14$), but here we list only the most important terms. Table II also shows the results obtained from first and second-order perturbation theory (PT). It can be seen that the fitted electrostatic terms agree very well with the PT

coefficients, in particular with the data calculated at the PT–RCCSD(T) level of theory. For the induction and dispersion terms we find some significant discrepancies, but the most important second-order fit coefficients (those with $n = 6$) show satisfactory agreement with PT–DFT. It should be noted that, for the fitted coefficients, no distinction can be made between induction and dispersion contributions. For the isotropic $C_{0,0,0,6}$ term, the PT-DFT calculations give a dispersion coefficient of 39.86 a.u. and an induction term of 6.99 a.u.

As an indication of the relative importance of the different $C_{L_A,L_B,L,n}$ coefficients, we explicitly give their contributions to the potential at $R = 30\ a_0$ (see Table II). These contributions, $V_{L_A,L_B,L,n}(R)$, were calculated as follows:

$$V_{L_A,L_B,L,n}(R) = N_{L_A,L_B,L} \frac{|C^{fit}_{L_A,L_B,L,n}|}{R^n}, \tag{10}$$

where $N_{L_A,L_B,L} = [4\pi/(2L_A + 1)(2L_B + 1)(2L + 1)]^{1/2}$ is the norm of the angular $A_{L_A,L_B,L}(\theta_A, \theta_B, \phi)$ functions. It is clear that the $n = 3$ dipole-dipole interaction dominates the potential by at least one order of magnitude, followed by the electrostatic dipole-quadrupole term. The main second order term is the isotropic $n = 6$ interaction, which, at 30 a_0, is still larger than the electrostatic $n = 5$ terms. The fact that the fitted $C_{1,1,2,3}$ and $C_{0,0,0,6}$ coefficients give the largest contributions in first and second order, respectively, indicates that the fit is not only numerical, but also physically meaningful. Thus, we may safely extrapolate the potential from 30 a_0 to larger R values.

Figure 2 shows the R-dependence of the fitted RCCSD(T) potential for two specific orientations $(\theta_A, \theta_B, \phi)$. For the linear geometry, with $\theta_A = \theta_B = \phi = 0°$, the leading dipole-dipole interaction is maximally attractive, while for $\theta_A = \theta_B = \phi = 90°$ the dipole-dipole term is zero. It can be seen that the $C_{1,1,2,3}$ coefficient dominates the long-range potential beyond $R \approx 12\ a_0$. Figure 2 also compares the total long-range expansion with the *ab initio* data, illustrating the region of validity of Eq. (7). It should be noted that, on the scale of the figure, the short-range expansion of Eq. (2) is indistinguishable from the total fitted potential of Eq. (9), and thus the short-range expansion is not explicitly shown. The long-range fit is very accurate for intermolecular distances larger than 8 a_0, which suggests that short-range (exchange and charge penetration) effects are only significant for $R \leq 8\ a_0$. This also justifies our choice of switching the potential from the short-range to the long-range expansion between 8 and 12 a_0.

B. Short-range potentials

Although the $S = 0$, 1, and 2 potentials obtained in this work are very similar to those reported by Dhont *et al.* [26], there are some notable differences at very short intermolecular distances. The differences are most pronounced at $R = 4.0\ a_0$, where the potentials exhibit the highest anisotropy. Figure 3 compares the two fit results for the quintet state as a function of θ_A and θ_B, with $R = 4.0\ a_0$ and $\phi = 0°$. Note that both surfaces were obtained from the same set of *ab initio* data. The fit of Ref. [26] shows more oscillatory behavior than our present result, in particular near $(\theta_A, \theta_B) = (180°, 150°)$ and $(30°, 0°)$. Furthermore, the potential of Dhont *et al.* has a local maximum around $(150°, 30°)$ that is clearly unphysical in nature. Similar patterns are found for the triplet and singlet states, as can be seen in Figs. 4 and 5. The $S = 0$ and 1 potentials of Ref. [26] exhibit more pronounced oscillations and local maxima, indicating more unphysical behavior. We therefore conclude that, in addition to the more accurate long-range potential, the fit of the short-range NH–NH potentials is also improved in the present work.

V. CONCLUSIONS AND OUTLOOK

We have constructed four-dimensional potential energy surfaces for the singlet, triplet, and quintet states of NH($^3\Sigma^-$) – NH($^3\Sigma^-$) based on high-level *ab initio* calculations. All potentials were fitted in terms of coupled spherical harmonics in the angular coordinates, and the long range was further expanded as a power series in $1/R$. Prior to fitting, the *ab initio* data were corrected for a size-consistency error of $0.5 \times 10^{-6}\ E_h$ occurring at the RCCSD(T) level of theory. The fitted long-range coefficients were found to be in good agreement with the results obtained from first and second-order perturbation theory.

Future work is planned to study the evaporative cooling process of NH, which requires knowledge of elastic and inelastic cross sections at (ultra)low temperatures. Rate constants and cross sections for (cold) reactive NH + NH collisions will also be calculated. Finally, we aim to explore the possibilities of cold controlled chemistry by investigating the influence of external fields.

Acknowledgments

We gratefully acknowledge Professor Robert Moszyński and Professor Hans-Joachim Werner for useful discussions on the RCCSD(T) size-consistency problem. LMCJ and GCG thank the Council for Chemical Sciences of the Netherlands Organization for Scientific Research (CW-NWO) for financial support. PSZ acknowledges EPSRC for funding the collaborative project CoPoMol under the ESF EUROCORES programme EuroQUAM.

APPENDIX

In this Appendix, we describe how we optimized the quadrature weights w_i for the integration of Legendre polynomials $P_l(x)$ on a given grid of mutually distinct points x_i $(i = 1, \ldots, n)$:

$$\int_{-1}^{1} P_l(x)dx = 2\delta_{l,0} \approx \sum_{i=1}^{n} w_i P_l(x_i). \tag{A.1}$$

We define the optimization as a minimization of the sum of square residuals $|\boldsymbol{r}|$:

$$|\boldsymbol{r}| = |\boldsymbol{A}\boldsymbol{w} - \boldsymbol{b}|, \tag{A.2}$$

where $\boldsymbol{A}$ is an $(l_{max} + 1) \times n$ matrix with elements $A_{li} = P_l(x_i)$ $(l = 0, \ldots, l_{max})$, $\boldsymbol{w}$ is a vector of length n containing the quadrature weights w_i, and $\boldsymbol{b}$ is a vector of length $l_{max} + 1$ with elements $b_l = 2\delta_{l,0}$. In the case of an n-point Gauss-Legendre quadrature, x_i and w_i are chosen in such a way that the integration is exact, i.e., $|\boldsymbol{r}| = 0$, for all polynomials up to degree $l_{max} = 2n-1$. For arbitrary, mutually distinct points x_i, we may calculate the weights as $\boldsymbol{w} = \boldsymbol{A}^{-1}\boldsymbol{b}$, since $\boldsymbol{A}$ is regular for $l_{max} = n - 1$ (see p. 145 of Ref. [32]). This results in a quadrature that is exact up to (at least) degree $n - 1$. Instead of using a quadrature that is exact for $l_{max} = n-1$ and most likely unsuitable for higher degree polynomials, we choose a compromise quadrature that is reasonable for $l_{max} > n-1$ at the expense of not being exact for lower degree polynomials. This may be achieved by linear least squares minimization of $|\boldsymbol{r}|$. However, we prefer to use a quadrature that is exact for constant functions $(l = 0)$, which requires a minimization of $|\boldsymbol{r}|$ with the constraint that $\sum_{i=1}^{n} w_i = 2$. For this purpose we take

$$\boldsymbol{w} = \boldsymbol{w}_0 + \boldsymbol{w}_\perp, \tag{A.3}$$

with $(\boldsymbol{w}_0)_i = 2/n$ for all $i = 1, \ldots, n$ and $\sum_{i=1}^{n} (\boldsymbol{w}_\perp)_i = 0$. This may be rewritten as $\boldsymbol{w}_0^T \boldsymbol{w}_\perp = 0$, with $\boldsymbol{w}_0^T$ denoting the transpose of $\boldsymbol{w}_0$. We can now expand $\boldsymbol{w}_\perp$ in an orthogonal basis $\{\boldsymbol{q}_i, i = 2, \ldots, n\}$ of vectors $\boldsymbol{q}_i$ that are perpendicular to $\boldsymbol{w}_0$:

$$\boldsymbol{w}_\perp = \sum_{i=2}^{n} \boldsymbol{q}_i c_i = \tilde{\boldsymbol{Q}} \boldsymbol{c}. \tag{A.4}$$

We observe that the first row of the matrix $\boldsymbol{A}$ is proportional to $\boldsymbol{w}_0$, and thus the vectors $\boldsymbol{q}_i$ can be generated by Gram-Schmidt QR-factorization of $\boldsymbol{A}^T$:

$$\boldsymbol{A}^T = \boldsymbol{Q}\boldsymbol{R}. \tag{A.5}$$

Here, $\boldsymbol{Q}$ is an $n \times n$ orthonormal matrix and $\boldsymbol{R}$ is an $n \times (l_{max} + 1)$ upper triangular matrix. The columns $i = 2, \ldots, n$ of $\boldsymbol{Q}$ form the matrix $\tilde{\boldsymbol{Q}}$ of Eq. (A.4). In order to find the expansion coefficients $\boldsymbol{c}$, we now remove the first row of $\boldsymbol{A}$ and the first element of $\boldsymbol{b}$, yielding the $(l_{max} \times n)$ matrix $\tilde{\boldsymbol{A}}$ and the null vector $\tilde{\boldsymbol{b}}$ of length l_{max}, respectively, and define the residual $\tilde{\boldsymbol{r}} = \tilde{\boldsymbol{A}}\boldsymbol{w}$. Substitution of Eq. (A.3) gives

$$|\tilde{\boldsymbol{r}}| = |\tilde{\boldsymbol{A}}\boldsymbol{w}_0 + \tilde{\boldsymbol{A}}\tilde{\boldsymbol{Q}}\boldsymbol{c}|, \tag{A.6}$$

which can be minimized in a standard least squares procedure to obtain the expansion coefficients $\boldsymbol{c}$. Finally, substitution of Eq. (A.4) into (A.3) gives the total optimal quadrature weights. In the present work, we have employed this method to generate optimal weights for the short-range quintet potential with $n = 11$ and $l_{max} = 16$.

---

[1] A. Micheli, G. K. Brennen, and P. Zoller, Nature Phys. **2**, 341 (2006).

[2] B. L. Lev, E. R. Meyer, E. R. Hudson, B. C. Sawyer, J. L. Bohn, and J. Ye, Phys. Rev. A **74**, 061402 (2006).

[3] H. L. Bethlem and W. Ubachs, Faraday Discuss. **142**, 25 (2009).

[4] M. R. Tarbutt, J. J. Hudson, B. E. Sauer, and E. A. Hinds, Faraday Discuss. **142**, 37 (2009).

[5] S. Y. T. van de Meerakker, N. Vanhaecke, M. P. J. van der Loo, G. C. Groenenboom, and G. Meijer, Phys. Rev. Lett. **95**, 013003 (2005), physics/0505097.

[6] J. J. Gilijamse, S. Hoekstra, S. Y. T. van de Meerakker, G. C. Groenenboom, and G. Meijer, Science **313**, 1617 (2006), `http://www.sciencemag.org/cgi/content/abstract/313/5793/1617`.

[7] J. J. Gilijamse, S. Hoekstra, S. A. Meek, M. Metsälä, S. Y. T. van de Meerakker, G. Meijer, and G. C. Groenenboom, J. Chem. Phys. **127**, 221102 (2007), 0710.2240.

[8] W. C. Campbell, G. C. Groenenboom, H.-I. Lu, E. Tsikata, and J. M. Doyle, Phys. Rev. Lett. **100**, 083003 (2008).

[9] R. V. Krems, Phys. Chem. Chem. Phys. **10**, 4079 (2008).

[10] D. DeMille, Phys. Rev. Lett. **88**, 067901 (2002).

[11] A. André, D. DeMille, J. M. Doyle, M. D. Lukin, S. E. Maxwell, P. Rabl, R. J. Schoelkopf, and P. Zoller, Nature Phys. **2**, 636 (2006).

[12] K. M. Jones, E. Tiesinga, P. D. Lett, and P. S. Julienne, Rev. Mod. Phys. **78**, 483 (2006).

[13] T. Köhler, K. Góral, and P. S. Julienne, Rev. Mod. Phys. **78**, 1311 (2006).

[14] H. L. Bethlem and G. Meijer, Int. Rev. Phys. Chem. **22**, 73 (2003).

[15] J. D. Weinstein, R. deCarvalho, T. Guillet, B. Friedrich, and J. M. Doyle, Nature **395**, 148 (1998).

[16] R. V. Krems, H. R. Sadeghpour, A. Dalgarno, D. Zgid, J. Kłos, and G. Chałasiński, Phys. Rev. A **68**, 51401 (2003).

[17] W. C. Campbell, E. Tsikata, H.-I. Lu, L. D. van Buuren, and J. M. Doyle, Phys. Rev. Lett. **98**, 213001 (2007).

[18] M. T. Hummon, W. C. Campbell, H.-I. Lu, E. Tsikata, Y. Wang, and J. M. Doyle, Phys. Rev. A **78**, 050702 (2008).

[19] S. Y. T. van de Meerakker, R. T. Jongma, H. L. Bethlem, and G. Meijer, Phys. Rev. A **64**, 041401 (2001).

[20] S. Hoekstra, M. Metsälä, P. C. Zieger, L. Scharfenberg, J. J. Gilijamse, G. Meijer, and S. Y. T. van de Meerakker, Phys. Rev. A **76**, 063408 (2007).

[21] N. Balakrishnan, G. C. Groenenboom, R. V. Krems, and A. Dalgarno, J. Chem. Phys. **118**, 7386 (2003).

[22] H. Cybulski, R. V. Krems, H. R. Sadeghpour, A. Dalgarno, J. Kłos, G. C. Groenenboom, A. van der Avoird, D. Zgid, and G. Chałasiński, J. Chem. Phys. **122**, 094307 (2005).

[23] C.-H. Lai, M.-D. Su, and S.-Y. Chu, J. Phys. Chem. A **107**, 2700 (2003).

[24] L. A. Poveda, M. Biczysko, and A. J. C. Varandas, J. Chem. Phys. **131**, 044309 (2009).

[25] M. Kajita, Phys. Rev. A **74**, 032710 (2006).

[26] G. S. F. Dhont, J. H. van Lenthe, G. C. Groenenboom, and A. van der Avoird, J. Chem.

Phys. **123**, 184302 (2005).

[27] P. J. Knowles, C. Hampel, and H.-J. Werner, J. Chem. Phys. **99**, 5219 (1993).

[28] P. J. Knowles, C. Hampel, and H.-J. Werner, J. Chem. Phys. **112**, E3106 (2000).

[29] S. F. Boys and F. Bernardi, Mol. Phys. **19**, 553 (1970).

[30] M. Heckert, O. Heun, J. Gauss, and P. G. Szalay, J. Chem. Phys. **124**, 124105 (2006).

[31] T. H. Dunning, J. Chem. Phys. **90**, 1007 (1989).

[32] J. Stoer and R. Bulirsch, *Introduction to Numerical Analysis* (Springer-Verlag, New York, 1980).

[33] K. P. Huber and G. Herzberg, *Molecular Spectra and Molecular Structure. IV. Constants of Diatomic Molecules* (Van Nostrand Reinhold, New York, 1979).

[34] MOLPRO is a package of *ab initio* programs written by H.-J. Werner and P. J. Knowles, with contributions from R. D. Amos, A. Berning, D. L.Cooper, M. J. O. Deegan, A. J. Dobbyn, F. Eckert, C. Hampel, T. Leininger, R. Lindh, A. W. Lloyd, W. Meyer, M. E. Mura, A. Nicklaß, P.Palmieri, K. Peterson, R. Pitzer, P. Pulay, G. Rauhut, M. Schütz, H. Stoll, A. J. Stone and T. Thorsteinsson.

[35] A. J. Stone, *The Theory of Intermolecular Forces* (Oxford University Press, Oxford, 1996).

[36] C. Adamo and V. Barone, J. Chem. Phys. **110**, 6158 (1999).

[37] *DALTON, a molecular electronic structure program, Release 2.0* (2005), http://www.kjemi.uio.no/software/dalton/dalton.html.

[38] D. J. Tozer and N. C. Handy, J. Chem. Phys. **109**, 10180 (1998).

[39] P. S. Żuchowski, R. Podeszwa, R. Moszyński, B. Jeziorski, and K. Szalewicz, J. Chem. Phys. **129**, 084101 (2008).

[40] A. J. Misquitta, R. Podeszwa, B. Jeziorski, and K. Szalewicz, J. Chem. Phys. **123**, 214103 (2005).

[41] P. S. Żuchowski, Chem. Phys. Lett. **450**, 203 (2008).

[42] R. Bukowski, W. Cencek, P. Jankowski, M. Jeziorska, B. Jeziorski, S. A. Kucharski, V. F. Lotrich, A. J. Misquitta, R. Moszyński, K. Patkowski, *et al.*, *SAPT2008: An* Ab Initio *Program for Many-Body Symmetry-Adapted Perturbation Theory Calculations of Intermolecular Interaction Energies*, University of Delaware and University of Warsaw (2008).

[43] P. E. S. Wormer and H. Hettema, *POLCOR package*, Nijmegen (1992).

[44] This g_4 option is, to our knowledge, not documented. The MOLPRO manual states that

"g_4 *makes CASPT2 calculations size extensive for cases in which a molecule dissociates to high-spin open-shell (RHF) atoms*".

[45] A. van der Avoird, P. E. S. Wormer, F. Mulder, and R. M. Berns, Top. Curr. Chem. **93**, 1 (1980).

[46] See EPAPS supplementary material at *** for the long-range and short-range fit coefficients of the quintet, triplet, and singlet potentials.

[47] A. N. Tikhonov and V. Y. Arsenin, *Solutions of Ill-Posed Problems* (Wiley, New York, 1977).

[48] T.-S. Ho and H. Rabitz, J. Chem. Phys. **104**, 2584 (1996).

[49] T.-S. Ho and H. Rabitz, J. Chem. Phys. **113**, 3960 (2000).

TABLE I: Size-consistency errors (ΔE) for the NH–NH system at the RCCSD and RCCSD(T) levels of theory. The basis sets correspond to the (aug)-cc-pVnZ (n = double, triple, quadruple, quintuple) sets of Dunning [31]. The errors are calculated as the difference between the energy of the separate monomers and the energy of the supersystem NH$\cdots$NH at an intermolecular distance of 30 000 a_0. All values are in 10^{-6} E_h.

Basis set	ΔE RCCSD	ΔE RCCSD(T)
cc-pVDZ	−3.15067	−0.50946
cc-pVTZ	−4.25041	−0.01069
cc-pVQZ	−4.70853	0.36976
cc-pV5Z	−4.92130	0.62672
aug-cc-pVDZ	−4.04159	0.01944
aug-cc-pVTZ	−4.88230	0.51290
aug-cc-pVQZ	−5.01375	0.68981
aug-cc-pV5Z	−5.03493	0.75827

TABLE II: Most important long-range coefficients obtained from the fit and from perturbation theory, and their contributions at 30 a_0. The order of importance is based on the value of n, and for each n only the four largest terms are given. Terms labeled with an asterisk are first-order (electrostatic) interactions. All values are in atomic units. Numbers in parentheses denote powers of 10.

L_A	L_B	L	n	$C^{fit}_{L_A,L_B,L,n}$	$C^{PT-RCCSD(T)}_{L_A,L_B,L,n}$	$C^{PT-DFT}_{L_A,L_B,L,n}$	$V_{L_A,L_B,L,n}(30\ a_0)$
1	1	2	3*	1.9697(+0)	1.9715(+0)	2.0127(+0)	3.8551(-05)
1	2	3	4*	-2.8394(+0)	-2.8597(+0)	-3.0642(+0)	1.2127(-06)
1	3	4	5*	1.6637(+1)	1.6761(+1)	1.7103(+1)	1.7654(-07)
2	2	4	5*	-5.6953(+0)	-5.4312(+0)	-6.1080(+0)	5.5389(-08)
0	0	0	6	4.7270(+1)		4.6852(+1)	2.2986(-07)
1	4	5	6*	-5.4131(+1)	-5.5049(+1)	-5.7422(+1)	1.5274(-08)
0	2	2	6	1.2657(+1)		1.5681(+1)	1.2309(-08)
2	3	5	6*	3.6904(+1)	3.9347(+1)	4.2140(+1)	9.1458(-09)
0	1	1	7	-1.8433(+2)		-8.2153(+1)	9.9596(-09)
1	2	3	7	-3.4979(+2)		1.5651(+1)	5.5331(-09)
0	3	3	7	-1.0784(+2)		-7.9522(+1)	2.4971(-09)
3	3	6	7*	3.1701(+2)	3.3946(+2)	3.4622(+2)	2.0359(-09)
0	0	0	8	9.2546(+2)		1.1077(+3)	5.0003(-09)
0	2	2	8	3.9371(+3)		1.4208(+3)	4.2544(-09)
1	1	2	8	4.5792(+3)		-1.0618(+2)	3.6882(-09)
2	2	4	8	-4.4826(+3)		6.2384(+2)	1.6146(-09)
0	1	1	9	3.0500(+4)		-3.1644(+3)	1.8310(-09)
1	2	3	9	9.9936(+4)		2.2929(+3)	1.7565(-09)
1	2	1	9	-2.3093(+4)		-6.1280(+2)	6.2000(-10)
0	3	3	9	9.0400(+3)		-5.6295(+3)	2.3259(-10)

FIG. 1: Isotropic part of the quintet potential calculated at the CCSD and CCSD(T) levels of theory. The data labeled "RCCSD" and "RCCSD(T)" correspond to the uncorrected spin-restricted data, "RCCSD-ΔE" and "RCCSD(T)-ΔE" to the size-consistency corrected data, and "UCCSD" and "UCCSD(T)" to the spin-unrestricted results.

FIG. 2: R-dependent quintet potential for two selected orientations $(\theta_A, \theta_B, \phi)$. The solid lines correspond to the total fitted potential, the dashed lines to the long-range potential, and the dotted lines to the long-range dipole-dipole interaction.

FIG. 3: (Color) Cuts of the quintet potential (in cm^{-1}) for $R = 4.0\ a_0$ and $\phi = 0°$. The left panel shows the fit obtained in this work and the right panel shows the results of Ref. [26].

FIG. 4: (Color) Cuts of the triplet potential (in cm^{-1}) for $R = 4.0\ a_0$ and $\phi = 0°$, calculated using Eq. (1). The upper panels correspond to the present work and the lower panels to the work of Dhont *et al.* [26].

FIG. 5: (Color) Cuts of the singlet potential (in cm^{-1}) for $R = 4.0\ a_0$ and $\phi = 0°$, calculated using Eq. (1). The upper panels correspond to the present work and the lower panels to the work of Dhont *et al.* [26].

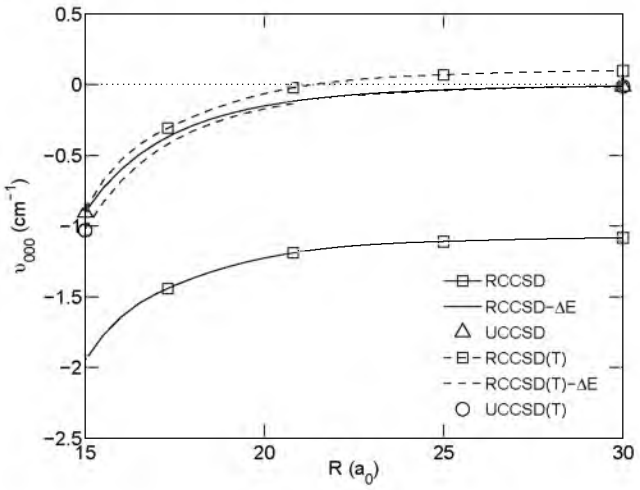

Janssen *et al.* Fig. 1.

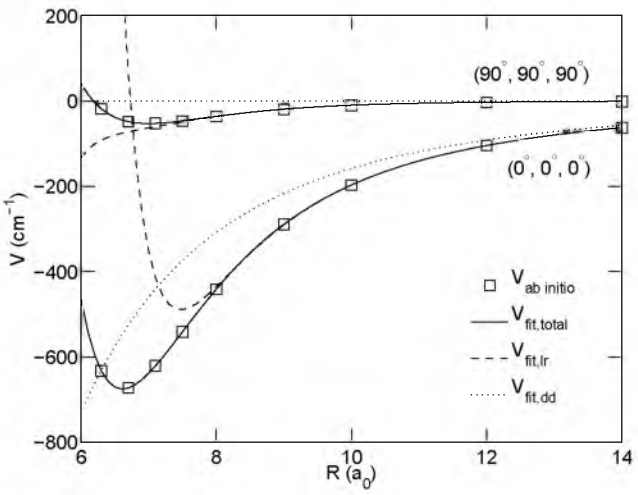

Janssen *et al.* Fig. 2.

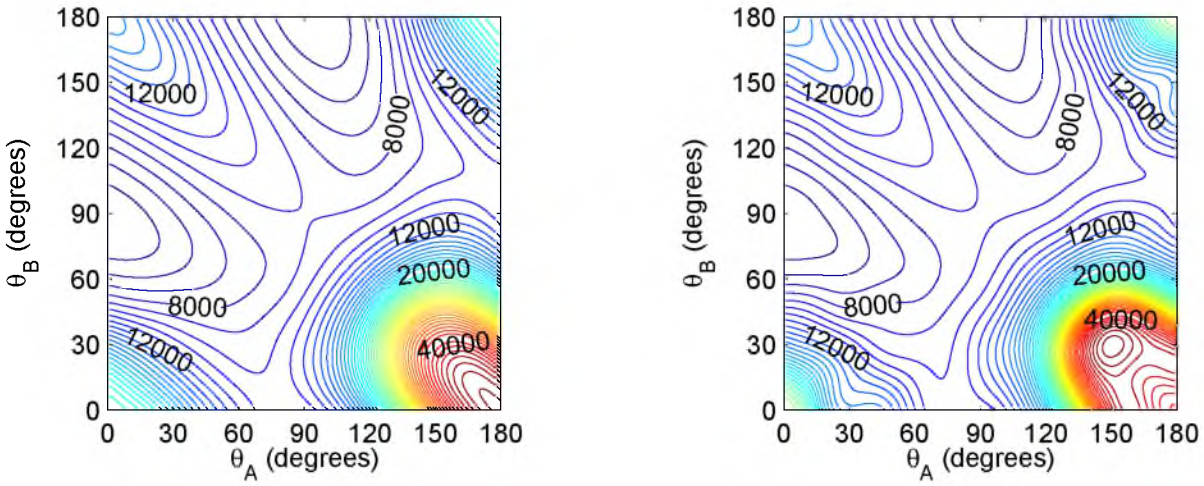

Janssen *et al.* Fig. 3.

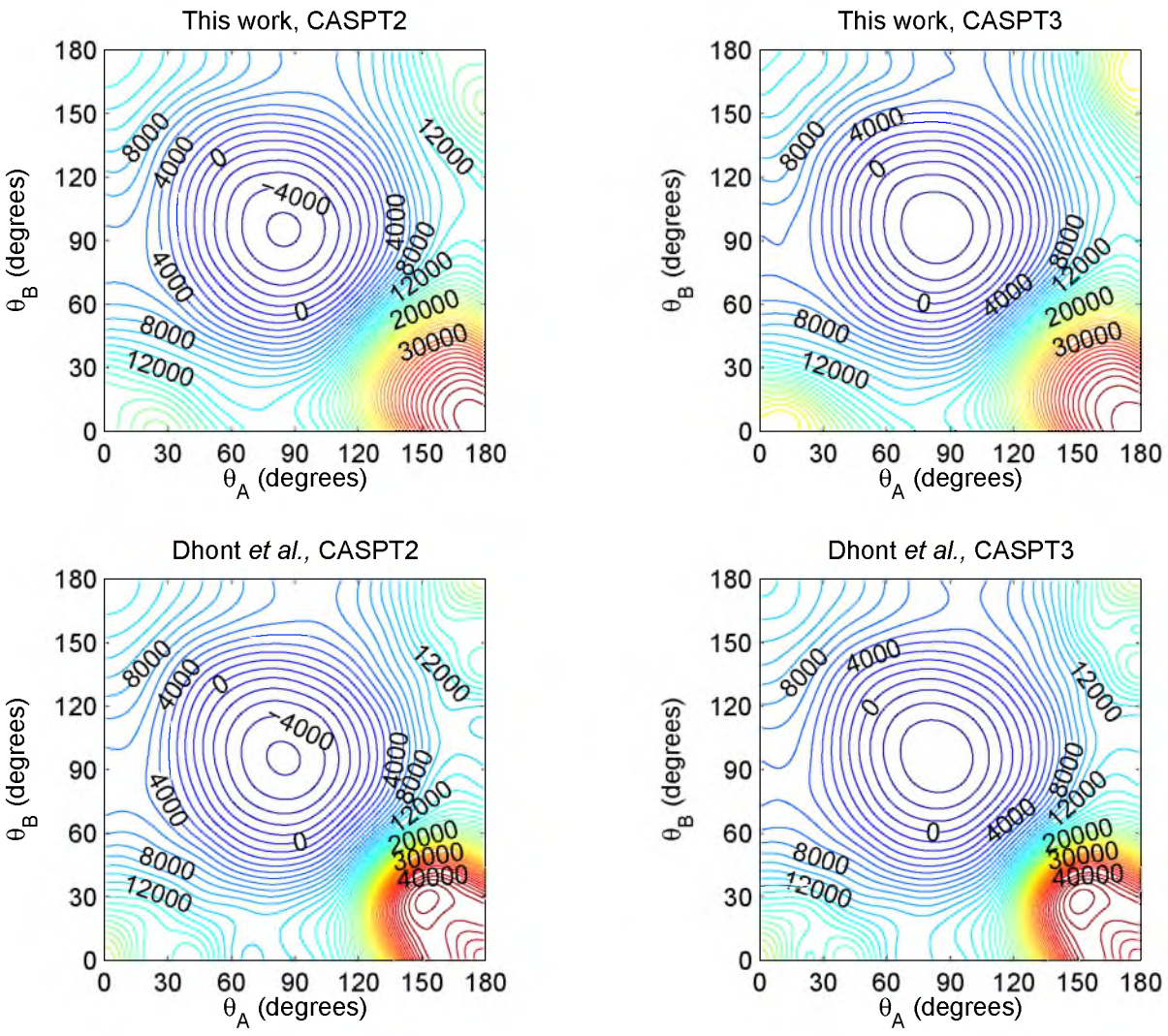

Janssen *et al.* Fig. 4.

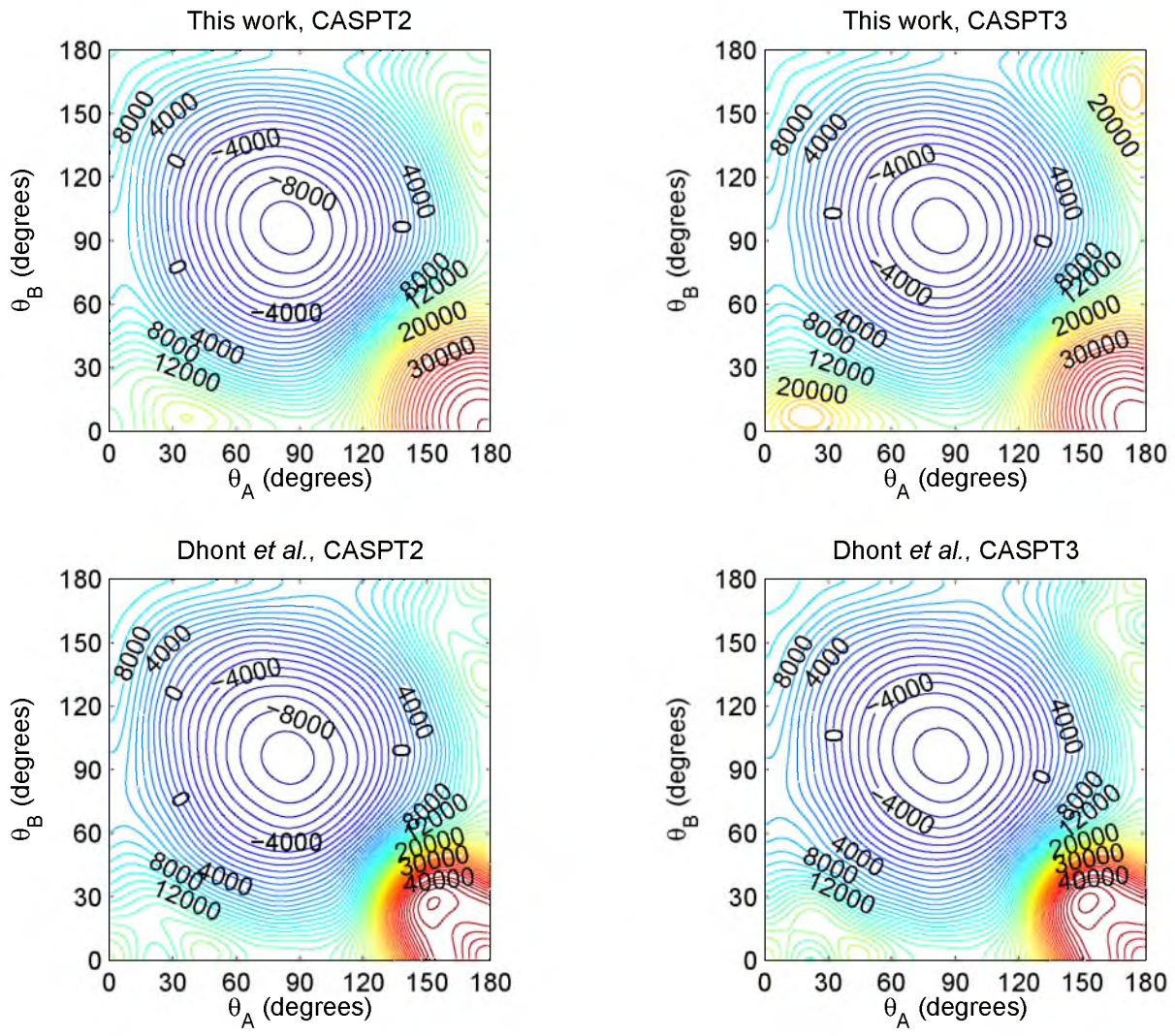

Janssen *et al.* Fig. 5.